Article

Molecular Cell

MicroRNA Clustering Assists Processing of Suboptimal MicroRNA Hairpins through the Action of the ERH Protein

Graphical Abstract

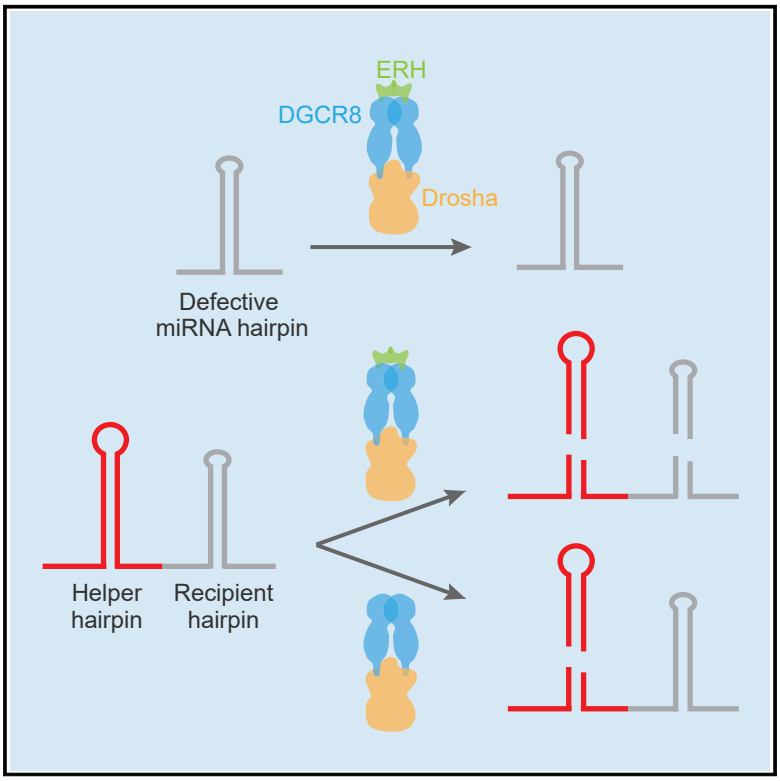

Highlights

- miRNA hairpins can assist in processing neighboring hairpins in mammalian cells
- The assistance scales with Microprocessor recognition of the linked helper hairpin
- Processing of the recipient hairpin is usually realized after processing of the helper
- ERH, which copurifies with Microprocessor, enables cluster assistance

Authors

Wenwen Fang, David P. Bartel

Correspondence

dbartel@wi.mit.edu

In Brief

MicroRNAs are processed from RNA hairpins. Multiple microRNA hairpins often reside in the same primary transcript. Fang and Bartel find that this clustered arrangement can enhance the processing of suboptimal hairpins in mammalian cells, and they identify ERH as a protein that both copurifies with Microprocessor and enables this cluster assistance.

Fang & Bartel, 2020, Molecular Cell *78*, 289–302
April 16, 2020
https://doi.org/10.1016/j.molcel.2020.01.026

CellPress

Molecular Cell
Article

MicroRNA Clustering Assists Processing of Suboptimal MicroRNA Hairpins through the Action of the ERH Protein

Wenwen Fang[1,2,3] and David P. Bartel[1,2,3,4,*]
[1]Howard Hughes Medical Institute, Cambridge, MA 02142, USA
[2]Whitehead Institute of Biomedical Research, Cambridge, MA 02142, USA
[3]Department of Biology, Massachusetts Institute of Technology, Cambridge, MA 02139, USA
[4]Lead Contact
*Correspondence: dbartel@wi.mit.edu
https://doi.org/10.1016/j.molcel.2020.01.026

SUMMARY

Microprocessor initiates the processing of microRNAs (miRNAs) from the hairpin regions of primary transcripts (pri-miRNAs). Pri-miRNAs often contain multiple miRNA hairpins, and this clustered arrangement can assist in the processing of otherwise defective hairpins. We find that miR-451, which derives from a hairpin with a suboptimal terminal loop and a suboptimal stem length, accumulates to 40-fold higher levels when clustered with a helper hairpin. This phenomenon tolerates changes in hairpin order, linker lengths, and the identities of the helper hairpin, the recipient hairpin, the linker-sequence, and the RNA polymerase that transcribes the hairpins. It can act reciprocally and need not occur co-transcriptionally. It requires Microprocessor recognition of the helper hairpin and linkage of the two hairpins, yet predominantly manifests after helper-hairpin processing. It also requires enhancer of rudimentary homolog (ERH), which copurifies with Microprocessor and can dimerize and interact with other proteins that can dimerize, suggesting a model in which one Microprocessor recruits another Microprocessor.

INTRODUCTION

MicroRNAs (miRNAs) are ~22-nt RNAs that direct the post-transcriptional repression of mRNAs. They act within a silencing complex, composed of an miRNA associated with an Argonaute (AGO) protein, in which the miRNA pairs to sites within target mRNAs and AGO mediates the repression of these mRNAs (Bartel, 2018). The human genome encodes hundreds of miRNAs, which collectively regulate mRNAs from most human genes (Friedman et al., 2009).

Canonical miRNAs of humans and other animals are transcribed by RNA polymerase II (Pol II) as part of longer primary transcripts (pri-miRNAs) (Lee et al., 2002, 2004; Cai et al., 2004). Each pri-miRNA has at least one region that folds back on itself to form an miRNA hairpin that is recognized by the Microprocessor, a heterotrimer complex that has one molecule of Drosha, an RNaseIII endonuclease, and two molecules of its co-factor DGCR8 (Nguyen et al., 2015). Drosha crops the hairpin about one helical turn from its base, leaving a staggered cut with a 2-nt 3′ overhang and releasing the precursor miRNA (pre-miRNA) (Figure 1A) (Lee et al., 2003; Han et al., 2006). The pre-miRNA is exported from the nucleus to the cytoplasm, where it undergoes a second processing step by Dicer (Grishok et al., 2001; Hutvágner et al., 2001; Lee et al., 2003). Dicer cleaves two helical turns from the base of the pre-miRNA to remove its loop and generate an miRNA duplex (Zhang et al., 2004), one strand of which is ultimately loaded onto AGO, forming the core silencing complex.

Some miRNA hairpins map within clusters in the genome, implying the production of multiple miRNAs from the same primary transcript (Lagos-Quintana et al., 2001; Lau et al., 2001). Recent analyses indicate that ~50% of conserved miRNA genes are clustered (<10 kb apart) in the human genome (Wang et al., 2016). Many of the clustered hairpins are related to one another, suggesting that some clusters are the result of tandem duplication of miRNA hairpins. However, in other cases, the clustered hairpins have no detectible similarities, suggesting that the clustering of miRNAs can impart an advantage, perhaps by facilitating coordinated expression (Lau et al., 2001; Lee et al., 2002; Aravin et al., 2003; Sempere et al., 2003; Baskerville and Bartel, 2005). In addition, a clustered arrangement seems to enhance the processing of some miRNAs, in that removal of neighboring hairpins can reduce their accumulation, as shown for one miRNA in a virus, two in the fly, and two in mouse (Feederle et al., 2011; Truscott et al., 2016; Lataniotis et al., 2017). Follow-up experiments investigating miR-11~998, one of the fly miRNA clusters, show that the accumulation of miR-998 is enhanced when miR-11 is placed either upstream or downstream of miR-998 or replaced by miR-1, and that this effect occurs at the step of Drosha processing (Truscott et al., 2016).

Of the many metazoan transcripts with the potential to fold back on themselves to form hairpins, relatively few are chosen as pri-miRNAs to enter the miRNA biogenesis pathway. The gatekeeper in this highly selective choice is the Microprocessor, which prefers hairpins with a stem of 35 ± 1 bp (tolerating several wobbles and mismatches) (Han et al., 2006; Fang and Bartel,

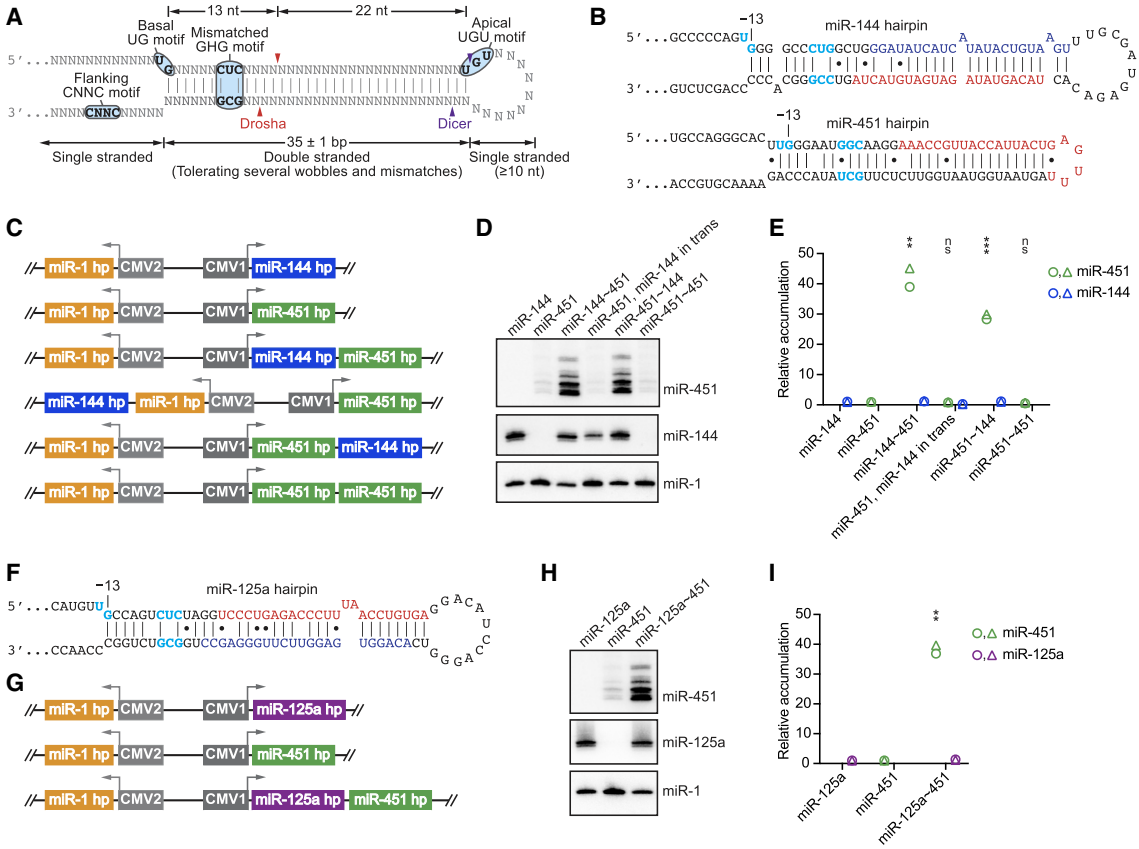

Figure 1. Cluster Assistance Enhances miR-451 Production

(A) Sequence and structural features that influence Microprocessor recognition and cleavage-site selection. Motifs are highlighted (blue). Redrawn from Fang and Bartel (2015).

(B) The human miR-144 and miR-451 hairpins used in the ectopic-expression experiments. Red letters indicate guide strands, blue letters indicate passenger strands, and cyan letters indicate matches to motifs that facilitate pri-miRNA processing.

(C) Schematics of the miRNA hairpin (hp) expression cassettes used in (D). Arrows indicate transcription start sites; CMV1 and CMV2 indicate two versions of the cytomegalovirus promoter.

(D) Northern blot analysis of miRNA accumulation from the indicated expression cassettes. Signal from incompletely resected miR-451 isoforms, which migrated more slowly than the fully resected isoform, was included in quantifications in (E) and all subsequent northern analyses.

(E) Quantification of (D) and its biological replicate (circles and triangles, respectively). For each lane, mature miRNA levels were first normalized to that of miR-1 and then to the levels from individually expressed miR-144 or miR-451 (mean of two replicates). Statistically significant or non-significant (ns) changes of miR-451 levels compared with the level of individually expressed miR-451 are indicated (**$p < 0.01$, ***$p < 0.001$, unpaired two-tailed t test).

(F) The human miR-125a hairpin, drawn as in (B).

(G) Schematics of the expression cassettes used in (H). Otherwise, this panel is as in (C).

(H) Northern blot analysis of miRNA accumulation from the indicated expression cassettes.

(I) Quantification of (H) and its biological replicate (circles and triangles, respectively). For each lane, mature miRNA levels were first normalized to miR-1 and then to the levels from individually expressed miR-125a or miR-451 (mean of two replicates). Statistically significant change of miR-451 level compared with the level of individually expressed miR-451 is indicated (**$p < 0.01$, unpaired two-tailed t test).

2015), an unstructured apical loop of ≥10 nt (Zeng et al., 2005), and single-stranded segments flanking the hairpin (Han et al., 2006) (Figure 1A). In addition to these structural features, four motifs, each located at specific positions relative to the processing site, can enhance processing efficiency and influence the site of processing (Figure 1A). These include three simple primary-sequence motifs, known as the basal UG motif, the apical UGU motif, and the flanking CNNC motif (Auyeung et al., 2013). The other motif is the mismatched GHG (mGHG), which is a complex primary- and secondary-structural motif involving six nucleotides of the basal stem (Fang and Bartel, 2015). The quality of a particular mGHG motif is best described using a score based on the ranked effect of each of the 4,096 nucleotide combinations at these six positions of the basal stem (Fang and Bartel, 2015; Kwon et al., 2019). Using these features, it is easy to design *de novo* pri-miRNA substrates that are processed efficiently by Microprocessor, even more efficiently than are natural pri-miRNAs (Fang and Bartel, 2015).

Because the features that Microprocessor uses to recognize an miRNA hairpin and crop it at the correct position can act redundantly to achieve the efficiency and accuracy needed in the cell, very few natural miRNA hairpins have an optimal set of

features (Fang and Bartel, 2015). Nonetheless, most evolutionarily conserved pri-miRNA hairpins possess a subset of the features sufficient for efficient and accurate processing. The miR-451 hairpin is a notable exception. Although it has two of the four motifs (an mGHG motif scoring in the top 1.5% and the basal UG motif), the miR-451 hairpin has very poor structural features, with a stem length of only 31 bp (counting from the paired G of its basal UG motif) and a loop size of only 4 nt (Figure 1B). These features are presumably important for pre-miR-451 to be processed in a Dicer-independent, non-canonical pathway involving loading of the pre-miRNA directly into AGO, followed by AGO-catalyzed slicing of one arm of the hairpin and poly(A)-specific ribonuclease (PARN)-mediated resection of the resulting 3′ end to generate an ~23-nt mature miRNA (Cheloufi et al., 2010; Cifuentes et al., 2010; Yang et al., 2010; Yoda et al., 2013).

Despite its unusually poor structural features, the miR-451 hairpin is a Microprocessor substrate (Cheloufi et al., 2010; Yang et al., 2010), and the mature miRNA becomes one of the most highly expressed miRNAs in erythroblasts and erythrocytes (Zhang et al., 2011; Juzenas et al., 2017). It accumulates to a level exceeding that of miR-144, which is transcribed on the same primary transcript but processed from a hairpin expected to be a good Microprocessor substrate, in that it has two motifs (an mGHG motif scoring in the top 0.6% and the basal UG motif) and nearly ideal structural features (Figure 1B). This ability of miR-451 to accumulate to the same level as miR-144 implies that it may have some unknown feature that compensates for its unusually poor structure. We set out to identify this feature and found that the miR-451 hairpin and some other defective mammalian miRNA hairpins can be efficiently processed if they are linked to a hairpin that can be efficiently processed on its own. Furthermore, we identify enhancer of rudimentary homolog (ERH) as a component of Microprocessor and show that it enables cluster-assisted processing of miR-451. This cluster assistance substantially increases the spectrum of pri-miRNAs that can be efficiently processed and motivates revision of the prevailing view of Microprocessor and substrate recognition.

RESULTS

Cluster Assistance Enhances miR-451 Production

When ectopically expressing miR-451 in HEK293 cells, we found that its accumulation was highly dependent on the context in which it was expressed. These experiments expressed the miRNAs of interest from a plasmid with a bidirectional promotor from which an miRNA of interest was transcribed in one direction and a control miRNA used to monitor plasmid transfection efficiency and miRNA recovery was transcribed in the opposite direction (Figure 1C). Compared to when miR-451 was expressed alone from its own transcript, its level increased ~40-fold when expressed from the same pri-miRNA transcript as miR-144 (Figures 1C–1E). In contrast, the accumulation of miR-144 did not change substantially when expressed from the same transcript as miR-451. The benefit of miR-144 on miR-451 accumulation was not observed when miR-144 was expressed from a different transcript, downstream of the miR-1 control miRNA (Figures 1C–1E), which disfavored a model in which the regulatory activity of miR-144 promotes miR-451 accumulation. As observed for miR-998 in flies (Truscott et al., 2016), the benefit remained when the order of the two miRNA hairpins within the pri-mRNA was switched (Figures 1C–1E) and when the helper hairpin was replaced with another efficiently processed miRNA hairpin, in our case that of miR-125a (Figures 1F–1I). However, the benefit was lost when the miR-144 hairpin was swapped with that of miR-451 (Figures 1C–1E). These results indicated that on its own, the miR-451 hairpin is a poorly recognized and poorly processed Microprocessor substrate, but when clustered on the same primary transcript with a more optimal neighboring miRNA hairpin, the miR-451 hairpin can become efficiently processed. We refer to this phenomenon as "cluster assistance," designating the miR-144 and miR-451 hairpins as helper and recipient hairpins, respectively.

Cluster Assistance Enhances the Processing of Other Mammalian miRNA Hairpins

To test whether cluster assistance could enhance the processing of other mammalian miRNA hairpins, we expanded our analysis to other clustered miRNAs. Similar to the miR-451 hairpin, the miR-181b-1 hairpin has a short stem and was thus predicted to be a suboptimal Microprocessor substrate and potential recipient of cluster assistance (Figure 2A). In the human genome, miR-181b-1 resides in a cluster with miR-181a-1, which is predicted to be a good Microprocessor substrate and thus a potential helper. Because miR-181a-1 and miR-181b-1 share sequence similarity that would confound northern analysis, we made an artificial cluster placing the miR-181b-1 hairpin in the same pri-miRNA as the miR-125a hairpin (Figures 2A and 2B). The accumulation of miR-181b-1 increased 20-fold when expressed in a cluster with miR-125a (Figures 2C and 2D). The accumulation of miR-125a decreased, perhaps because of competition for downstream factors such as Dicer and AGO as the miR-181b-1 level increased (Figures 2C and 2D). The other cluster tested was miR-374b~421. Although the miR-374b hairpin, with its short basal stem and small apical loop, was predicted to be the recipient of cluster assistance, both miRNAs accumulated to higher levels when expressed from a cluster (Figures 2E–2H). The effect size was also smaller than those observed for the other clusters. Nonetheless, our results for pri-miR-374b~421 indicated that cluster assistance can benefit multiple members in the same pri-miRNA and that it can act reciprocally, with the same hairpins acting as both helpers and recipients.

Further Characterization of Cluster Assistance

To test the hypothesis that the accumulation of the recipient miRNA depends on efficient Microprocessor recognition of its helper hairpin, we mutated the basal stem of the miR-144 hairpin to make this hairpin a less optimal Microprocessor substrate. When the basal stem of the miR-144 hairpin was shortened by 5 bp (Figure 3A, miR-144m1), accumulation of miR-144 decreased, and so did that of miR-451 (Figures 3B and 3C). When compensatory mutations restored the optimal basal stem length of the miR-144 hairpin (Figure 3A, miR-144m2), the levels of mature miR-144 and miR-451 were both restored

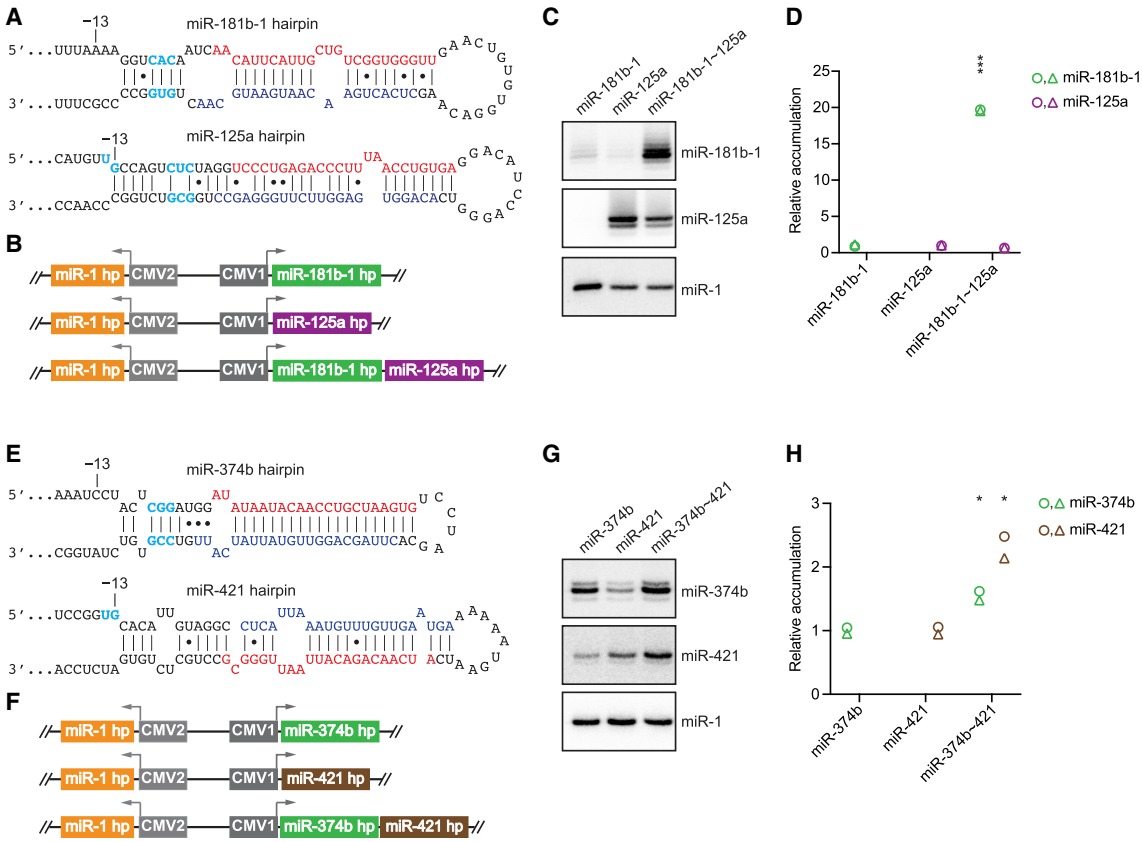

Figure 2. Cluster Assistance Enhances Processing of Other Mammalian miRNA Hairpins

(A) The human miRNA hairpins used in the overexpression experiments in (C). Otherwise, this panel is as in Figure 1B.

(B) Schematics of the expression cassettes used in (C). Otherwise, this panel is as in Figure 1C.

(C) Northern blot analysis of miRNA accumulation from the indicated expression cassettes.

(D) Quantification of (C) and its biological replicate (circles and triangles, respectively). For each lane, mature miRNA levels were first normalized to that of miR-1 and then to the levels from individually expressed miR-181b-1 or miR-125a (mean of two replicates). Statistically significant change of miR-181b-1 level compared with the level of individually expressed miR-181b-1 is indicated (***$p < 0.001$, unpaired two-tailed t test).

(E) The human miRNA hairpins used in the overexpression experiments in (G). Otherwise, this panel is as in Figure 1B.

(F) Schematics of the expression cassettes used in (G). Otherwise, this panel is as in Figure 1C.

(G) Northern blot analysis of miRNA accumulation from the indicated expression cassettes.

(H) Quantification of (G) and its biological replicate (circles and triangles, respectively). For each lane, mature miRNA levels were first normalized to that of miR-1 and then to the levels from individually expressed miR-374b or miR-421 (mean of two replicates). Statistically significant changes in miR-374b and miR-421 levels compared with the levels of individually expressed miRNAs are indicated (*$p < 0.05$, unpaired two-tailed t test).

(Figures 3B and 3C). Likewise, when the basal stem of the miR-144 hairpin was lengthened by 5 bp (Figure 3A, miR-144m3, m4), the accumulation of miR-144 and miR-451 both decreased, whereas when simultaneous mutations restored the optimal basal stem length of the miR-144 hairpin (Figure 3A, miR-144m5), the levels of miR-144 and miR-451 were both restored (Figures 3B and 3C). These striking differences in miR-451 accumulation observed as a consequence of mutations predicted to affect Microprocessor recognition of the neighboring miR-144 hairpin indicated that efficient processing of the miR-451 hairpin depends on recognition of its helper hairpin.

To explore how the spacing between the helper and recipient miRNA hairpins can influence cluster assistance, we increased the length of the linker region between the miR-144 and miR-451 hairpins. Exogenous sequences from either *nanoLuc* mRNA or yeast *ski2* mRNA were inserted to increase this linker from 95 nt in the human miR-144∼451 pri-miRNA transcript to 309, 909, and 3,072 nt (Figure 3D). At each of these linker lengths, cluster assistance was retained, although the magnitude of the effect dropped 3-fold when the length increased to 3,072 nt (Figures 3E and 3F). These results indicated that cluster assistance can efficiently operate over long linker lengths (1 kb), but can diminish when the distance becomes too long.

Microprocessor is reported to interact with Pol II (Gromak et al., 2013; Church et al., 2017), raising the possibility that Pol II may help mediate cluster assistance. To test this possibility, we expressed the miR-144∼451 cluster under the control of the U6 promoter (Figure 3G), which directs Pol III transcription. Cluster assistance was still observed but was somewhat diminished (Figures 3H–3J), which indicated that it does not require

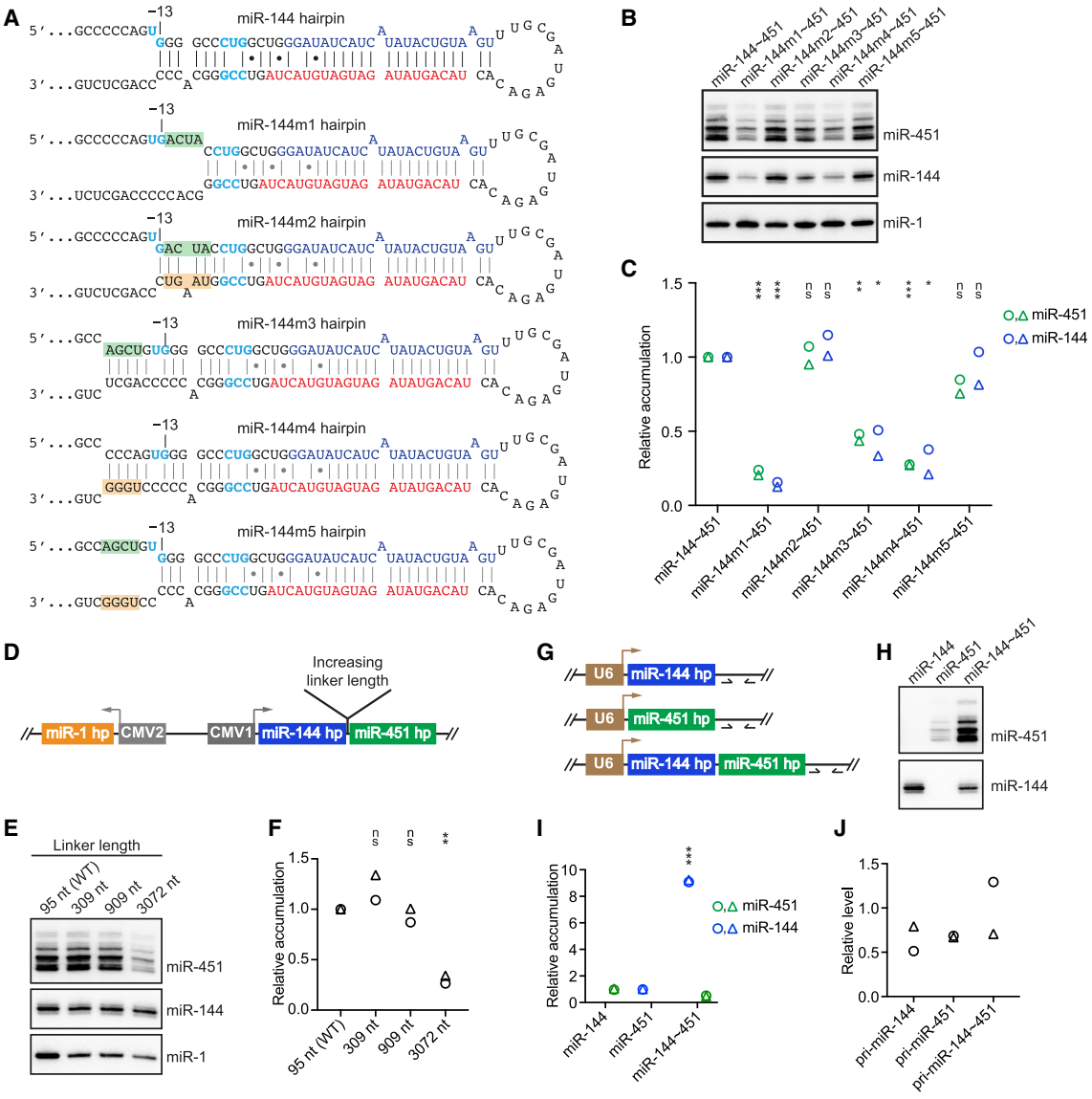

Figure 3. Further Characterization of Cluster Assistance

(A) The miR-144 wild-type (WT) and mutant hairpins (m1–m5) designed to test whether cluster assistance depends on efficient recognition of the helper hairpin. Mutations introduced in the basal stem of the miR-144 hairpin are shaded by green and orange boxes. Otherwise, this panel is as in Figure 1B.

(B) Northern blot analysis of miRNA accumulation from the indicated expression cassettes that encoded derivatives of the miR-144 hairpin shown in (A).

(C) Quantification of (B) and its biological replicate (circles and triangles, respectively). For each lane, mature miRNA levels were first normalized to that of miR-1 and then to the levels from the miR-144~451 construct. Statistically significant or non-significant (ns) changes in miR-144 or miR-451 levels compared with levels for the WT cluster are indicated (*$p < 0.05$, **$p < 0.01$, ***$p < 0.001$, unpaired two-tailed t test).

(D) Schematic of the expression cassettes used in (E) to test the sensitivity of cluster assistance to the spacing of the two hairpins. Otherwise, this panel is as in Figure 1C.

(E) Northern blot analyses of miRNA accumulation from expression cassettes that had sequences of the indicated lengths linking the miR-144 and miR-451 hairpins.

(F) Quantification of (E) and its biological replicate (circles and triangles, respectively). For each lane, the level of miRNA-451 was normalized to that of miR-144, and the level from the WT sample was set to 1 (**$p < 0.01$, unpaired two-tailed t test). This normalization provided a conservative quantification of cluster assistance at longer linker lengths; if normalizing instead to miR-1 levels, then miR-451 expression from the construct with a 3,072-nt linker would have equaled that from the construct with the WT linker.

(G) Schematics of the expression cassettes used in (H) to test whether cluster assistance requires Pol II transcription. U6 indicates the U6 promoter. Arrows downstream of the miRNA hairpins indicate qPCR primers used to assay pri-miRNA expression.

(H) Northern blot analysis of miRNA accumulation from the indicated U6-driven expression cassettes of (G).

(legend continued on next page)

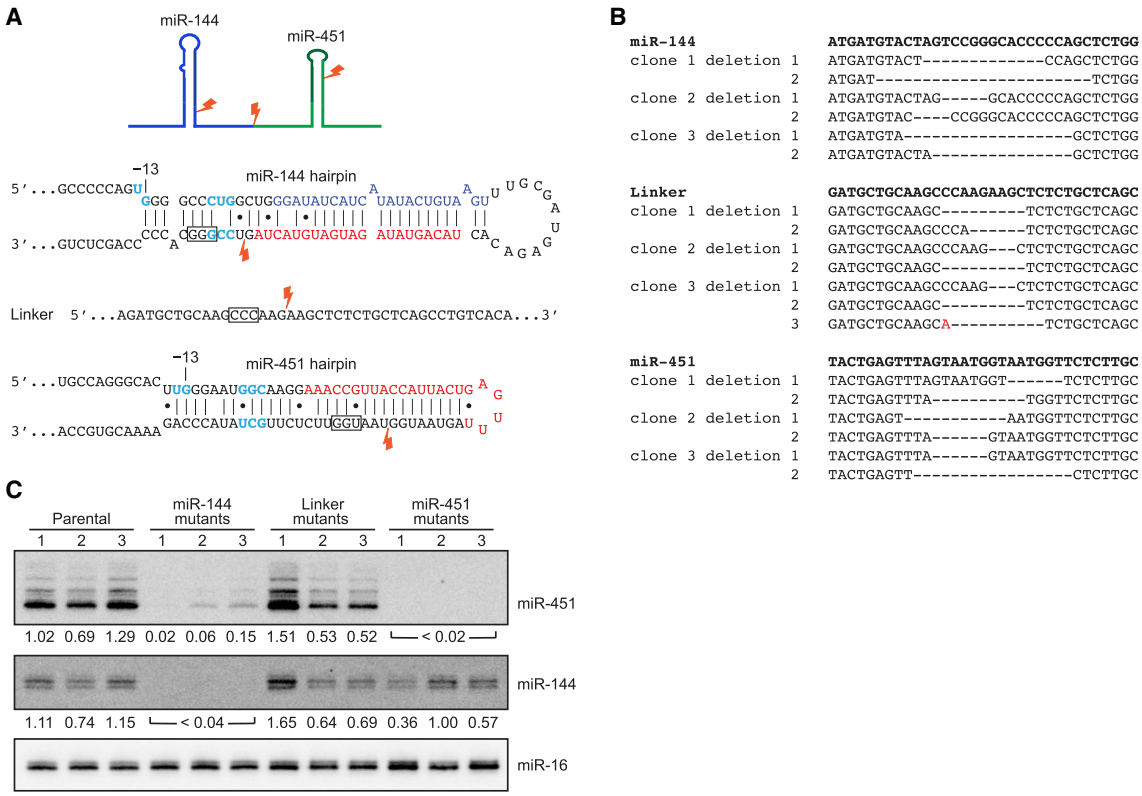

Figure 4. Cluster Assistance Acts on miRNAs Expressed from Their Endogenous Loci

(A) Diagrams showing the Cas9 cut sites (lightning bolts) in the miR-144~451 cluster. Boxes indicate protospacer adjacent motif (PAM) sequences. Otherwise, this panel is as in Figure 1B.

(B) Sequence alignments of WT (bold) and mutant alleles from indicated clonal cell lines. Deleted nucleotides are indicated by dashes. An inserted nucleotide is colored in red.

(C) Northern blot analysis of miRNA accumulation from the indicated clonal cell lines. Normalized levels are shown below each lane. For each lane, levels of miR-451 and miR-144 were first normalized to that of miR-16, and then to the mean of the relative levels from the three parental cell lines.

Pol II transcription, although we cannot rule out a role for Pol II in contributing to the efficiency of the effect.

Cluster Assistance Acts on the miR-451 Hairpin Expressed from Its Endogenous Locus

The previously identified example of cluster assistance was discovered by looking at the effects of deleting miR-11 in flies (Truscott et al., 2016), and other suspected cases of cluster assistance were observed after disruption of a presumed helper gene in its endogenous context (Feederle et al., 2011; Lataniotis et al., 2017). To confirm that cluster assistance of miR-451 can also occur when the miRNAs are expressed under physiological conditions from their chromosomal context, we used Cas9 to introduce local deletions in the miR-144~451 cluster in K562 cells, which endogenously express this cluster. The guide RNAs (gRNAs) directed cleavage within loci encoding either the miR-144 hairpin, the linker region between the miR-144 and miR-451 hairpins, or the miR-451 hairpin (Figure 4A). For each gRNA, three clonal cell lines with deletions at each allele were generated (Figure 4B). Three clonal cell lines derived from the parental K562 cells were also generated as controls. In the cell lines with deletions in the linker region, accumulation of both miR-451 and miR-144 resembled that observed in the control parental lines (Figure 4C). In cell lines in which the miR-451 hairpin was disrupted, miR-451 accumulation was affected, but miR-144 accumulation was not substantially affected, whereas in cell lines in which the miR-144 hairpin was disrupted, a substantial reduction in miR-451 accumulation accompanied the reduced miR-144 accumulation (Figure 4C). These results mirrored those observed in our plasmid-based ectopic-expression experiments, confirming that for these miRNAs expressed from their endogenous loci, the accumulation of miR-451

(I) Quantification of (H) and its biological replicate (circles and triangles, respectively). Mature miRNA levels from the individually expressed cassettes (mean of two replicates) were set to 1 (***$p < 0.001$, unpaired two-tailed t test).

(J) RT-qPCR analysis of pri-miRNA expression in Drosha knockout cells, using primers indicated in (G). *GAPDH* mRNA was used as an internal control, and the average level of pri-miR-144~451 was set to 1. Shown is quantification of the two biological replicates (circles and triangles); no statistically significant difference was observed ($p > 0.05$, unpaired two-tailed t test).

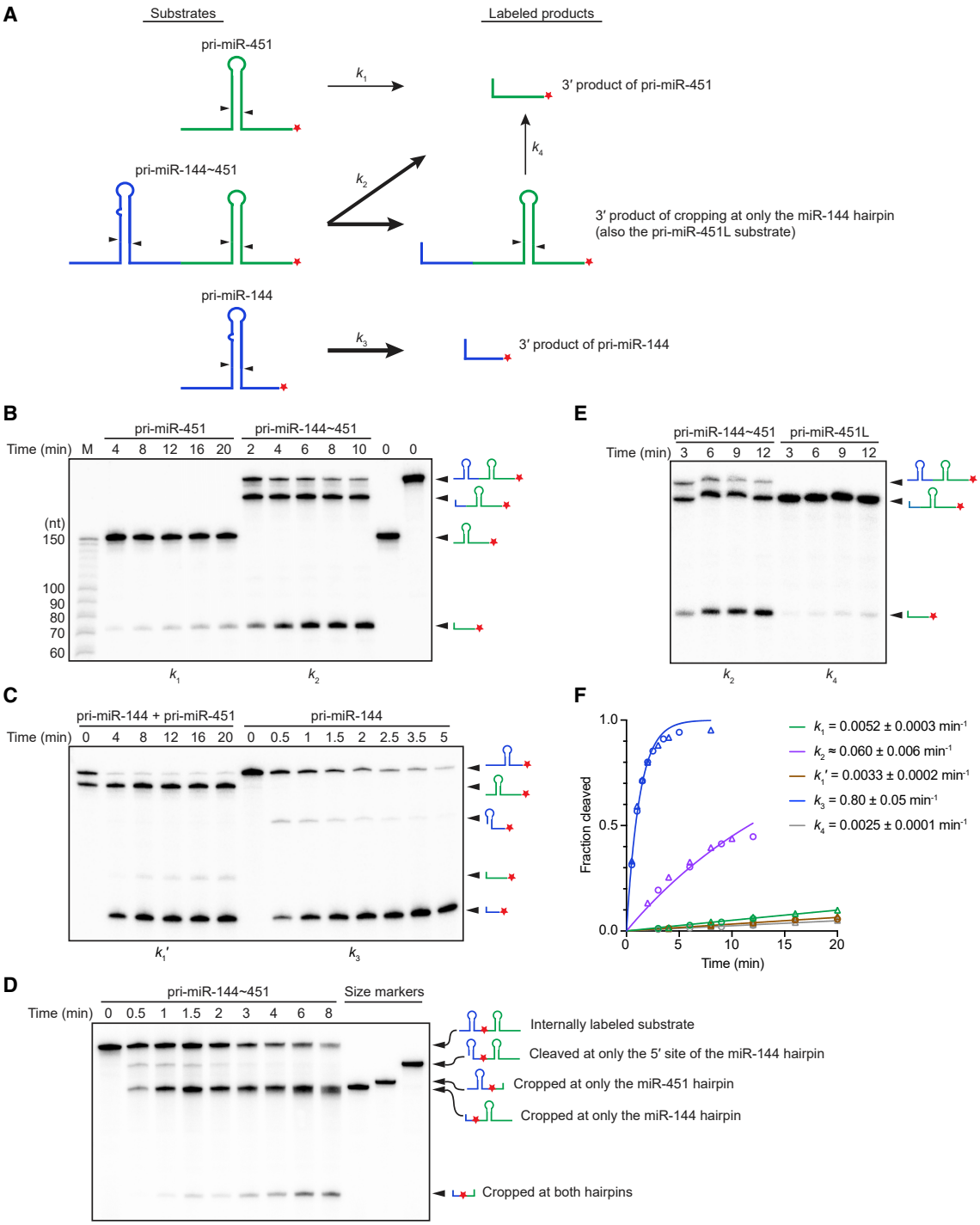

Figure 5. Cluster Assistance Acts at the Level of pri-miRNA Processing

(A) Diagrams showing the substrates and labeled products of *in vitro* processing experiments. The red star indicates the 3′ radiolabel, the arrowheads indicate Drosha cleavage sites, and the arrows indicate processing reactions yielding radiolabeled products with corresponding rate constants (k_1–k_4) labeled. Note that k_2 represents the rate constant of miR-451 hairpin processing in a context in which it benefits from cluster assistance, even if the miR-144 hairpin has already been processed, whereas k_4 represents the rate constant of the disassociated product of miR-144 hairpin processing, which did not benefit from cluster assistance.

(B) Processing assays of pri-miR-451 and pri-miR-144~451 using a lysate made from cells overexpressing Microprocessor. For comparison, markers (M) and substrates that had not been incubated with lysate (0 min) were also loaded. Below each time course, the rate constant calculated using results from that time course and its replicate is indicated.

(C) Processing assays of pri-miR-451 with pri-miR-144 added in *trans* and pri-miR-144. Otherwise, this panel is as in (B).

(legend continued on next page)

depends on its clustered expression with miR-144, but not vice versa.

Cluster Assistance Acts at the Level of pri-miRNA Processing

To this point our analyses used northern blots to assay mature miRNA accumulation, which is a function of the efficiencies of multiple biogenesis steps as well as degradation. To isolate the step of pri-miRNA processing, we performed processing assays *in vitro*, using lysate from cells that overexpressed Microprocessor (Drosha and DGCR8) (Auyeung et al., 2013) and radiolabeled pri-miRNA substrates (Figure 5A). As expected from our results in cells, the processing of the miR-451 hairpin was substantially faster when in a cluster with miR-144 (Figure 5B), with an ~12-fold enhancement in the processing rate constant (compare k_1 and k_2 in Figure 5F). Further supporting our model of cluster assistance, more rapid processing was not observed when the miR-144 hairpin was supplied on a separate transcript (compare k_1 and k_1' in Figures 5B, 5C, and 5F).

Despite its large influence, cluster assistance was unable to enhance the processing rate of the miR-451 hairpin to the point that reached that of the miR-144 hairpin (compare k_2 and k_3, Figures 5B, 5C, and 5F). However, substantially enhanced processing of the miR-451 hairpin was observed after 4 min, a time at which only 20% of pri-miR-144~451 was intact (Figures 5B and 5F), which indicated that cluster assistance can be realized even after the helper hairpin is processed. When we followed processing of an internally labeled pri-miR-144~451 substrate, we did not observe an intermediate in which only the miR-451 hairpin was cropped, confirming that for most pri-miRNA molecules, the miR-144 hairpin was processed before that of miR-451 (Figure 5D). The slow processing of a pri-miR-451 substrate that extended up to the 3′ cleavage site of the miR-144 hairpin, thereby mimicking the 3′ product of cropping at only the miR-144 hairpin in the pri-miR-144~451 substrate, showed that the region that remained covalently attached to the miR-451 hairpin was insufficient to mediate cluster assistance (compare k_4 with k_1 and k_2 in Figures 5B, 5E, and 5F). These results suggested that portions of the miR-144 hairpin upstream of the cropping product were able to mediate cluster assistance, despite no longer being covalently linked to the miR-451 hairpin when cluster assistance manifested as enhanced miR-451 processing. The ability of cluster assistance to operate after miR-144 hairpin cropping allowed the processing product of the miR-451 hairpin to reach approximately half that of the miR-144 hairpin by 10 min, despite being produced with a 13-fold slower rate constant (Figures 5B, 5C, and 5F).

The miR-451 Hairpin Requires Cluster Assistance Because of Its Short Hairpin and Small Loop

Using the *in vitro* system, we also investigated why the miR-451 hairpin is not processed efficiently on its own. When lengthening its stem from 31 bp to the 35 bp optimum, the processing rate did not increase substantially, and when extending the apical loop from 4 to 12 nt, the processing rate increased only 7-fold (Figure 6). However, when both the stem and the loop were extended to their more optimal lengths, the processing rate constant increased 170-fold and resembled that of the miR-144 hairpin (Figures 5F and 6). These results indicated that both the short stem and the small loop explain why the miR-451 hairpin requires cluster assistance for efficient processing, with the benefit of lengthening its stem contingent on also having a more suitable loop.

ERH Copurifies with Microprocessor and Helps Mediate Cluster Assistance

To acquire additional insight into the mechanism of cluster assistance, we searched for molecular players that help mediate this effect. We considered a model in which the intrinsically disordered N-terminal region of Drosha mediates dimerization or high-order assembly of the Microprocessor complex, such that binding of the helper hairpin could promote binding of a second Microprocessor to the recipient hairpin. To test this model, we assayed the processing of the miR-451 hairpin either on its own (pri-miR-451) or in the cluster context (pri-miR-144~451) using lysates that overexpressed either full-length Drosha or N-terminally truncated Drosha (D390), in which the first 389 amino acids of Drosha had been removed. Although the processing rates of the miR-451 hairpin, either on its own or in the clustered context, decreased when using D390 rather than full-length Drosha, cluster assistance was still observed with D390, indicating that the N-terminal region of Drosha is dispensable for cluster assistance (Figure 7A).

Our use of lysates that overexpress Microprocessor in the *in vitro* assays left open the possibility that factors other than Drosha and DGCR8 may help mediate cluster assistance. Cluster assistance was not observed when we performed processing assays with affinity-purified Microprocessor, but it was restored when we added lysate made from Drosha, DGCR8 double-knockout cells (Figures 7B and 7C), suggesting that at least one additional factor contributed by the lysate was required to mediate cluster assistance. Accordingly, we initiated experiments to identify this factor, but before completing these experiments, we were informed by Sabastian Herzog that his lab had discovered that scaffold attachment factor B (SAFB) proteins enable cluster-assisted accumulation of miR-15a and other miRNAs (Hutter et al., 2019).

We found the involvement of SAFB1 and SAFB2 particularly intriguing because ERH, a known interacting protein of SAFB1/2 (Drakouli et al., 2017), also interacts with Microprocessor (Kavanaugh et al., 2015). We had observed that despite its small size of only 12 kDa, ERH was easily detected in highly purified preparations of Microprocessor. For example, a substantial

(D) Processing assays of internally labeled pri-miR-144~451 using a lysate made from cells overexpressing Microprocessor. Standards representing potential processing intermediates were also loaded (size markers). The red star indicates an internally radiolabeled phosphate.
(E) Processing assays of pri-miR-144~451 and pri-miR-451L. Otherwise, this panel is as in (B).
(F) Quantification of (B), (C), and (E) and their independent replicates (circles and triangles, respectively). The line for each substrate represents the best fit of all of the data to an exponential reaction course, which generated the observed rate constants (k, shown ± 95% confidence intervals). k_2 is an approximation due to a small contribution from k_4.

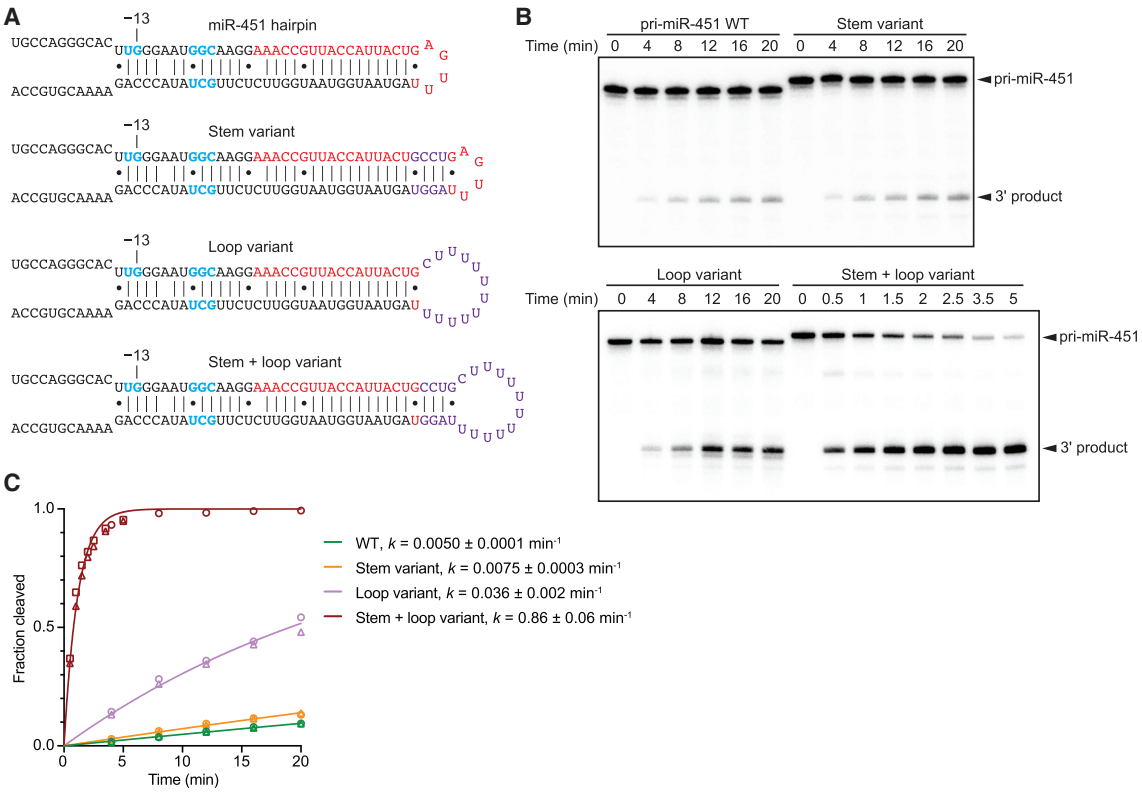

Figure 6. The miR-451 Hairpin Requires Cluster Assistance for Efficient Processing Because of Its Short Hairpin and Small Loop

(A) The miR-451 hairpin and its variants. Purple letters indicate nucleotides added to the apical stem or replacing the loop. Otherwise, this panel is as in Figure 1B.

(B) Processing assays of pri-miR-451 and its variants. The 0 min samples were not incubated with lysate.

(C) Quantification of (B) and its replicates. Two independent replicates (circles and triangles) were performed on each substrate, except for the stem + loop variant, for which a third replicate was performed (squares). Otherwise, this panel is as in Figure 5F.

amount of ERH copurified with Microprocessor that had been through two rounds of affinity purification: the first was an immunopurification of FLAG-tagged Drosha (D390-TN), which had been overexpressed together with DGCR8 in mammalian cells, and the second was based on affinity to a pri-miRNA substrate (Figure 7D). In addition, ERH continued to associate with Microprocessor when further purified on a gel-filtration column (Figure 7E). These results indicated that ERH could be a tightly associated accessory factor—or perhaps even core constituent—of Microprocessor, which was not detected in previous purifications because of its unusually small size.

Reasoning that SAFB proteins may mediate cluster assistance through their interaction with ERH, we tested whether ERH was also required for cluster assistance. Using doxycycline-inducible CRISPR interference (Gilbert et al., 2014), we knocked down ERH using two different gRNAs in K562 cells (Figure 7F). Although a strong growth phenotype was observed after knockdown with each of the two gRNAs, consistent with a critical role for ERH in the cell cycle (Weng and Luo, 2013), cells could be cultured for 5 d after inducing knockdown. Assaying accumulation of the pri-miR-451 hairpin by RT-qPCR showed that at 4 d post-knockdown, it accumulated to a level ~15-fold higher than that observed in control cells in which knockdown was not induced (Figure 7G). In contrast, little difference was observed for accumulation of the miR-144 hairpin, indicating that ERH knockdown specifically affected the processing of miR-451 and not miR-144 (Figure 7G).

To analyze mature miRNA accumulation, we performed high-throughput sequencing of small RNAs from control and 5 d knockdown samples and analyzed the expression change of each clustered miRNA compared with the average expression change of other members of its cluster. Among the 38 clustered miRNAs passing our expression threshold (≥100 reads in each of the two control replicates), miR-451 and miR-144 were the most differentially affected miRNAs upon ERH knockdown, with a 2.3-fold lower ratio of miR-451:miR-144 observed in the ERH knockdown compared to control cells (Figure 7H; Table S1; p = 0.00062, t test). The observation that the magnitude of the effect of ERH knockdown was lower when examining mature miRNA accumulation than when examining hairpin accumulation was expected because mature mammalian miRNAs can have half-lives of days (Kingston and Bartel, 2019), whereas pri-miRNAs are presumably more transient, and thus mature miRNA levels are expected to take much longer to reach a new equilibrium. With respect to other proposed recipients of cluster assistance, the expression of miR-181b was not high enough in K562 cells to pass our expression threshold, and signals for miR-374b and

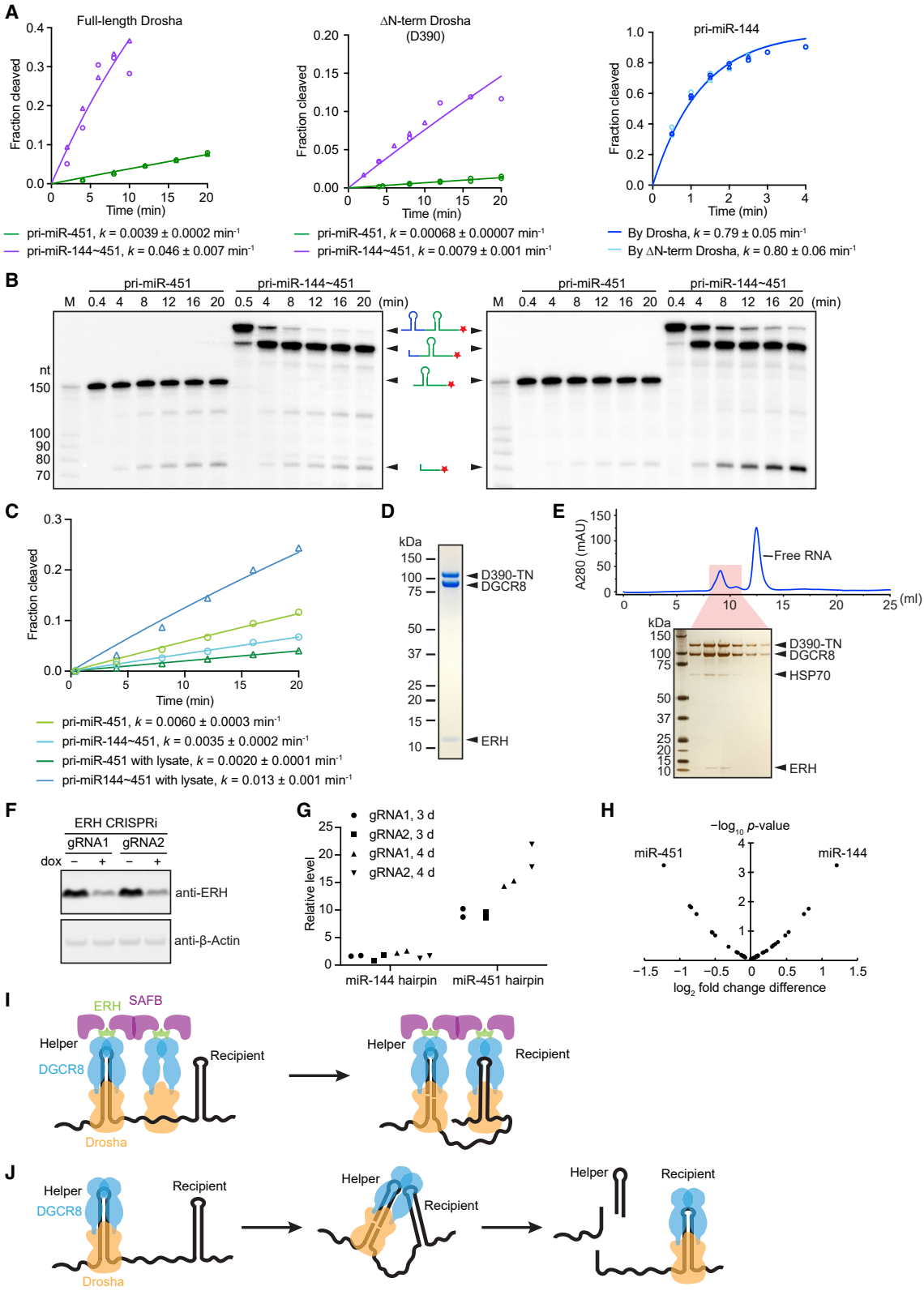

(legend on next page)

miR-421 were also not expected because both miRNAs of the cluster are recipients of cluster assistance.

DISCUSSION

We show that efficient processing of the miR-451 hairpin and other suboptimal miRNA hairpins relies on a more optimal hairpin residing in the same pri-miRNA. This cluster assistance is *cis*-acting, as miRNA-144 provided in *trans* did not promote miR-451 biogenesis *in vivo* (Figures 1C–1E) or *in vitro* (Figures 5C and 5F). Previous observations of mutations in the miR-145 hairpin affecting miRNA accumulation from the neighboring miR-143 hairpin or mutations in miR-195 hairpin affecting miRNA accumulation from the neighboring miR-497 hairpin are attributed to an influence on structural accessibility (Lataniotis et al., 2017). However, we show that cluster assistance is robust against changes in the ordering of the hairpins, the identity of the helper and recipient hairpins, and the identity and length of the linker separating the hairpins (Figures 1, 2, and 3). Moreover, the effect is reduced when the helper hairpin is either shortened or extended (Figures 3A–3C). These results, some of which had also been observed in the study of miR-998 accumulation in flies (Truscott et al., 2016), argue against the idea that differential structural accessibility explains cluster assistance. Moreover, our observation of cluster assistance of miRNA hairpins that were either transcribed by Pol III in cells (Figures 3G–3J) or premade *in vitro* (Figure 5) ruled out a required role for Pol II or any co-transcriptional process.

So, how does cluster assistance work? Mutations designed to affect Microprocessor recognition of only the helper hairpin have an equally severe effect on the processing of the recipient hairpin (Figures 3A–3C), which shows that the mechanism involves Microprocessor recognition of the helper hairpin. However, the helper hairpin cannot act as a magnet to attract Microprocessor, and thus the simple increase in Microprocessor local concentration imparted by helper-hairpin binding cannot explain cluster assistance. Without data to the contrary, the present model of Microprocessor substrate recognition reasonably assumes that the complex acts in isolation and binds to only one hairpin at a time, such that binding one hairpin excludes binding of the other (Fang and Bartel, 2015; Kwon et al. (2016); Nguyen et al., 2015). Under this mutually exclusive model, the increase in local concentration imparted by helper-hairpin binding would be fully negated by the fact that it cannot interact with the recipient hairpin when it is bound to the helper hairpin, and thus the presence of the helper hairpin could not increase the probability of Microprocessor diffusing to the recipient hairpin. Therefore, to explain cluster assistance, the prevailing model of Microprocessor substrate recognition must be revised to allow for binding of the recipient hairpin before full release of the helper hairpin or its products.

Two alternative revisions of the prevailing model would enable cluster assistance (Figures 7I and 7J). The first invokes dimerization or multimerization of Microprocessors. In this scenario, Microprocessor recognition of the helper hairpin would bring another Microprocessor to the vicinity of the recipient hairpin, thereby enhancing its processing (Figure 7I). In the other potential revision to the model of Microprocessor substrate recognition, a single Microprocessor complex recognizes the recipient hairpin before fully dissociating from the helper hairpin or its products. For example, the recipient hairpin could displace the

Figure 7. ERH Copurifies with Microprocessor and Helps Mediate Cluster Assistance

(A) Analysis of the effects of the Drosha N-terminal region. Shown are analyses of the processing rates of the miR-451 hairpin when this hairpin was either alone (pri-miR-451) or together with the miR-144 hairpin (pri-miR-144~451), using a lysate made from cells overexpressing DGCR8 and either full-length Drosha (left) or N-terminally truncated Drosha (D390, center). Also shown for comparison are analyses of the processing rates of the miR-144 hairpin when using a lysate made from cells overexpressing DGCR8 and either full-length Drosha or N-terminally truncated Drosha (right). Otherwise, this panel is as in Figure 5F.

(B) Assays of pri-miR-451 and pri-miR-144~451 processing using either affinity-purified Microprocessor (left) or affinity-purified Microprocessor supplemented with a lysate made from cells lacking both Drosha and DGCR8 (right).

(C) Quantification of miR-451 hairpin processing from (B). Otherwise, this panel is as in Figure 5F.

(D) Analysis of proteins that copurify with Microprocessor. FLAG-tagged D390-TN, the N-terminally truncated version of Drosha that also had active-site mutations that conferred a *trans*-dominant negative phenotype (Heo et al., 2008), was overexpressed in Expi293F cells with DGCR8, FLAG-affinity purified, incubated with ATP to remove HSP70 chaperones, and further purified by affinity to a desthiobiotin-tagged pri-miRNA. Proteins were separated on an SDS-PAGE and visualized using GelCode Blue Stain. Other than D390-TN and DGCR8, the only other protein detected migrated at ~12 kDa and was identified as ERH by mass spectrometry.

(E) Migration of ERH with Microprocessor on a gel-filtration column. Microprocessor was purified as in (D), except that the HSP70 chaperones were not washed away, and then was run on a Superdex 200 Increase size-exclusion column. Six consecutive fractions that represented the shaded region of the chromatogram were separated on an SDS-PAGE and then silver stained.

(F) Western blot confirming knockdown of ERH 3 d after inducing CRISPRi in cells expressing each of the two gRNAs (lanes 2 and 4, respectively). β-Actin was probed as a loading control.

(G) RT-qPCR analysis of the levels of unprocessed miR-144 and miR-451 hairpins after inducing ERH knockdown for either 3 or 4 d. All of the values were first normalized to that of the control mRNA (*GAPDH*), and then each value observed after CRISPRi induction was normalized to that observed in the corresponding cells for which knockdown was not induced.

(H) Analysis of small-RNA sequencing of ERH knockdown and control cells. The change in the expression of each clustered miRNA upon ERH knockdown was compared to that of the geometric average of the other member(s) from the same cluster. Points for miRNAs with significant changes in relative expression are labeled (t test, $p < 0.01$). See also Table S1.

(I) Model for the mechanism of cluster assistance. Microprocessors form a dimer (or higher-order assembly) of complexes through the action of both ERH, which stably associates with Microprocessor, and SAFB, which can both interact with ERH and dimerize. Binding of one Microprocessor to the helper hairpin increases the propensity of the other Microprocessor to bind the recipient hairpin.

(J) Alternative model for the mechanism of cluster assistance. After binding and cleaving the helper hairpin, Microprocessor remains associated with the helper hairpin (or its processing product) in a way that allows it to begin to recognize the recipient hairpin. ERH and SAFB, which enable cluster assistance, would play roles in this model, but are not drawn because the nature of these roles is unclear.

helper hairpin in a stepwise manner involving an intermediate in which both hairpins are partially bound (Figure 7J), perhaps enabled by the divergently facing double-stranded RNA-binding domains of DGCR8 (Sohn et al., 2007).

The discoveries that SAFB and ERH are each required for cluster assistance (Hutter et al., 2019) (Figures 7G and 7H) favor the first scenario, which involves the association of Microprocessors. Because SAFB can both dimerize (Townson et al., 2003) and interact with ERH (Drakouli et al., 2017), while ERH can both dimerize (Arai et al., 2005; Wan et al., 2005) and interact with Microprocessor (Figures 7D and 7E) (Kavanaugh et al., 2015), together, these two proteins might mediate the association of two or more Microprocessors, thereby explaining how the binding of the helper hairpin could bring a second Microprocessor to the vicinity of the recipient hairpin (Figure 7I).

Another critical mechanistic feature of cluster assistance is its ability to operate even after the helper hairpin is cleaved (Figure 5). This ability, which presumably results from the continued association of the Microprocessor with its processing products, dramatically increases the utility of cluster assistance. For example, without this ability, the 13-fold difference in processing rates observed between the miR-144 and clustered miR-451 hairpins would imply that no more than 8% of the miR-451 hairpin could be processed with help from cluster assistance. However, the ability of this assistance to operate after miR-144 hairpin cropping substantially increases this percentage, thereby explaining why over half of the hairpin is processed with help from cluster assistance (Figure 5F).

In addition to these mechanistic ramifications, our results support the idea that previous results should be reevaluated in light of cluster assistance. For example, when considering the effects of miRNA knockouts, knowledge of cluster assistance increases the impetus to examine the possibility that the knockout may influence miRNA accumulation from neighboring hairpins (Feederle et al., 2011; Truscott et al., 2016; Lataniotis et al., 2017). Moreover, in our previous experiments testing the roles of the four miRNA motifs, the effect of deleting the motif seemed muted when assayed in cells compared to when assayed *in vitro* (Auyeung et al., 2013; Fang and Bartel, 2015). This difference can now be understood in light of cluster assistance—when testing in cells, the influence of each motif is examined using constructs in which the control hairpin resides on the same primary transcript and thus can impart cluster assistance, whereas *in vitro*, the control hairpin is added as a separate RNA.

The phenomenon of cluster assistance also has evolutionary implications, helping to explain why miRNA clusters are so prevalent. When a new miRNA hairpin emerges near an existing hairpin, cluster assistance may enable it to be efficiently processed even before it acquires all of the features required for optimal processing. This effect may also buffer mutations in recently established hairpins, thereby relieving some constraints on the evolution of mature miRNA sequences and facilitating more rapid expansion and functional adaptation of miRNAs in the cluster.

STAR★METHODS

Detailed methods are provided in the online version of this paper and include the following:

SUPPLEMENTAL INFORMATION

Supplemental Information can be found online at https://doi.org/10.1016/j.molcel.2020.01.026.

ACKNOWLEDGMENTS

We thank S. Gu for the Drosha knockout and Drosha, DGCR8 double-knockout HEK293T cells; V.N. Kim, T. Tuschl, F. Zhang, and J.S. Weissman for plasmids; K. Shen and S. McGeary, T. Eisen, K. Xiang, and other members of the Bartel lab for helpful discussions; the Whitehead Institute fluorescence-activated cell sorting (FACS) facility for cell sorting; the Whitehead Proteomics Facility for mass spectrometry analyses; and the Whitehead Genome Technology Core for small-RNA sequencing. This research was supported by the NIH (K99GM123230, to W.F., and R35GM118135, to D.P.B). D.P.B. is an investigator at the Howard Hughes Medical Institute.

AUTHOR CONTRIBUTIONS

W.F. and D.P.B conceived the project, designed the study, and wrote the manuscript. W.F. performed the experiments.

DECLARATION OF INTERESTS

The authors declare no competing interests.

Received: July 19, 2019
Revised: January 2, 2020
Accepted: January 27, 2020
Published: April 16, 2020

REFERENCES

Arai, R., Kukimoto-Niino, M., Uda-Tochio, H., Morita, S., Uchikubo-Kamo, T., Akasaka, R., Etou, Y., Hayashizaki, Y., Kigawa, T., Terada, T., et al. (2005). Crystal structure of an enhancer of rudimentary homolog (ERH) at 2.1 Angstroms resolution. Protein Sci. *14*, 1888–1893.

Aravin, A.A., Lagos-Quintana, M., Yalcin, A., Zavolan, M., Marks, D., Snyder, B., Gaasterland, T., Meyer, J., and Tuschl, T. (2003). The small RNA profile during *Drosophila melanogaster* development. Dev. Cell *5*, 337–350.

Auyeung, V.C., Ulitsky, I., McGeary, S.E., and Bartel, D.P. (2013). Beyond secondary structure: primary-sequence determinants license pri-miRNA hairpins for processing. Cell *152*, 844–858.

Bartel, D.P. (2018). Metazoan MicroRNAs. Cell *173*, 20–51.

Baskerville, S., and Bartel, D.P. (2005). Microarray profiling of microRNAs reveals frequent coexpression with neighboring miRNAs and host genes. RNA *11*, 241–247.

Cai, X., Hagedorn, C.H., and Cullen, B.R. (2004). Human microRNAs are processed from capped, polyadenylated transcripts that can also function as mRNAs. RNA *10*, 1957–1966.

Cheloufi, S., Dos Santos, C.O., Chong, M.M., and Hannon, G.J. (2010). A Dicer-independent miRNA biogenesis pathway that requires Ago catalysis. Nature *465*, 584–589.

Church, V.A., Pressman, S., Isaji, M., Truscott, M., Cizmecioglu, N.T., Buratowski, S., Frolov, M.V., and Carthew, R.W. (2017). Microprocessor recruitment to elongating RNA Polymerase II is required for differential expression of microRNAs. Cell Rep. *20*, 3123–3134.

Cifuentes, D., Xue, H., Taylor, D.W., Patnode, H., Mishima, Y., Cheloufi, S., Ma, E., Mane, S., Hannon, G.J., Lawson, N.D., et al. (2010). A novel miRNA processing pathway independent of Dicer requires Argonaute2 catalytic activity. Science *328*, 1694–1698.

Dai, L., Chen, K., Youngren, B., Kulina, J., Yang, A., Guo, Z., Li, J., Yu, P., and Gu, S. (2016). Cytoplasmic Drosha activity generated by alternative splicing. Nucleic Acids Res. *44*, 10454–10466.

Drakouli, S., Lyberopoulou, A., Papathanassiou, M., Mylonis, I., and Georgatsou, E. (2017). Enhancer of rudimentary homologue interacts with scaffold attachment factor B at the nuclear matrix to regulate SR protein phosphorylation. FEBS J. *284*, 2482–2500.

Fang, W., and Bartel, D.P. (2015). The menu of features that define primary microRNAs and enable de novo design of microRNA Genes. Mol. Cell *60*, 131–145.

Feederle, R., Haar, J., Bernhardt, K., Linnstaedt, S.D., Bannert, H., Lips, H., Cullen, B.R., and Delecluse, H.J. (2011). The members of an Epstein-Barr virus microRNA cluster cooperate to transform B lymphocytes. J. Virol. *85*, 9801–9810.

Friedman, R.C., Farh, K.K., Burge, C.B., and Bartel, D.P. (2009). Most mammalian mRNAs are conserved targets of microRNAs. Genome Res. *19*, 92–105.

Fromm, B., Domanska, D., Hoye, E., Ovchinnikov, V., Kang, W., Aparicio-Puerta, E., Johansen, M., Flatmark, K., Mathelier, A., Hovig, E., and et al. (2020). MirGeneDB 2.0: the metazoan microRNA complement. Nucleic Acids Res. *48* (D1), D132–D141.

Gilbert, L.A., Horlbeck, M.A., Adamson, B., Villalta, J.E., Chen, Y., Whitehead, E.H., Guimaraes, C., Panning, B., Ploegh, H.L., Bassik, M.C., et al. (2014). Genome-scale CRISPR-mediated control of gene repression and activation. Cell *159*, 647–661.

Grishok, A., Pasquinelli, A.E., Conte, D., Li, N., Parrish, S., Ha, I., Baillie, D.L., Fire, A., Ruvkun, G., and Mello, C.C. (2001). Genes and mechanisms related to RNA interference regulate expression of the small temporal RNAs that control *C. elegans* developmental timing. Cell *106*, 23–34.

Gromak, N., Dienstbier, M., Macias, S., Plass, M., Eyras, E., Cáceres, J.F., and Proudfoot, N.J. (2013). Drosha regulates gene expression independently of RNA cleavage function. Cell Rep. *5*, 1499–1510.

Han, J., Lee, Y., Yeom, K.H., Kim, Y.K., Jin, H., and Kim, V.N. (2004). The Drosha-DGCR8 complex in primary microRNA processing. Genes Dev. *18*, 3016–3027.

Han, J., Lee, Y., Yeom, K.H., Nam, J.W., Heo, I., Rhee, J.K., Sohn, S.Y., Cho, Y., Zhang, B.T., and Kim, V.N. (2006). Molecular basis for the recognition of primary microRNAs by the Drosha-DGCR8 complex. Cell *125*, 887–901.

Heo, I., Joo, C., Cho, J., Ha, M., Han, J., and Kim, V.N. (2008). Lin28 mediates the terminal uridylation of *let-7* precursor MicroRNA. Mol. Cell *32*, 276–284.

Hutter, K., Lohmüller, M., Jukic, A., Eichin, F., Avci, S., Labi, V., Hoser, S.M., Hüttenhofer, A., Villunger, A., and Herzog, S. (2019). SAFB2 enables the processing of suboptimal stem-loop structures in clustered primary miRNA transcripts. bioRxiv. https://doi.org/10.1101/858647.

Hutvágner, G., McLachlan, J., Pasquinelli, A.E., Bálint, E., Tuschl, T., and Zamore, P.D. (2001). A cellular function for the RNA-interference enzyme Dicer in the maturation of the let-7 small temporal RNA. Science *293*, 834–838.

Juzenas, S., Venkatesh, G., Hübenthal, M., Hoeppner, M.P., Du, Z.G., Paulsen, M., Rosenstiel, P., Senger, P., Hofmann-Apitius, M., Keller, A., et al. (2017). A comprehensive, cell specific microRNA catalogue of human peripheral blood. Nucleic Acids Res. *45*, 9290–9301.

Kavanaugh, G., Zhao, R., Guo, Y., Mohni, K.N., Glick, G., Lacy, M.E., Hutson, M.S., Ascano, M., and Cortez, D. (2015). Enhancer of rudimentary homolog affects the replication stress response through regulation of RNA processing. Mol. Cell. Biol. *35*, 2979–2990.

Kingston, E.R., and Bartel, D.P. (2019). Global analyses of the dynamics of mammalian microRNA metabolism. Genome Res. *29*, 1777–1790.

Kwon, S.C., Baek, S.C., Choi, Y.G., Yang, J., Lee, Y.S., Woo, J.S., and Kim, V.N. (2019). Molecular basis for the single-nucleotide precision of primary microRNA processing. Mol. Cell *73*, 505–518.e5.

Kwon, S.C., Nguyen, T.A., Choi, Y.G., Jo, M.H., Hohng, S., Kim, V.N., and Woo, J.S. (2016). Structure of human DROSHA. Cell *164*, 81–90.

Lagos-Quintana, M., Rauhut, R., Lendeckel, W., and Tuschl, T. (2001). Identification of novel genes coding for small expressed RNAs. Science *294*, 853–858.

Landthaler, M., Yalcin, A., and Tuschl, T. (2004). The human DiGeorge syndrome critical region gene 8 and its *D. melanogaster* homolog are required for miRNA biogenesis. Curr. Biol. *14*, 2162–2167.

Lataniotis, L., Albrecht, A., Kok, F.O., Monfries, C.A.L., Benedetti, L., Lawson, N.D., Hughes, S.M., Steinhofel, K., Mayr, M., and Zampetaki, A. (2017). CRISPR/Cas9 editing reveals novel mechanisms of clustered microRNA regulation and function. Sci. Rep. *7*, 8585.

Lau, N.C., Lim, L.P., Weinstein, E.G., and Bartel, D.P. (2001). An abundant class of tiny RNAs with probable regulatory roles in *Caenorhabditis elegans*. Science *294*, 858–862.

Lee, Y., Jeon, K., Lee, J.T., Kim, S., and Kim, V.N. (2002). MicroRNA maturation: stepwise processing and subcellular localization. EMBO J. *21*, 4663–4670.

Lee, Y., Ahn, C., Han, J., Choi, H., Kim, J., Yim, J., Lee, J., Provost, P., Rådmark, O., Kim, S., and Kim, V.N. (2003). The nuclear RNase III Drosha initiates microRNA processing. Nature *425*, 415–419.

Lee, Y., Kim, M., Han, J., Yeom, K.H., Lee, S., Baek, S.H., and Kim, V.N. (2004). MicroRNA genes are transcribed by RNA polymerase II. EMBO J. *23*, 4051–4060.

Nguyen, T.A., Jo, M.H., Choi, Y.G., Park, J., Kwon, S.C., Hohng, S., Kim, V.N., and Woo, J.S. (2015). Functional anatomy of the human Microprocessor. Cell *161*, 1374–1387.

Sempere, L.F., Sokol, N.S., Dubrovsky, E.B., Berger, E.M., and Ambros, V. (2003). Temporal regulation of microRNA expression in *Drosophila melanogaster* mediated by hormonal signals and broad-Complex gene activity. Dev. Biol. *259*, 9–18.

Shalem, O., Sanjana, N.E., Hartenian, E., Shi, X., Scott, D.A., Mikkelson, T., Heckl, D., Ebert, B.L., Root, D.E., Doench, J.G., and Zhang, F. (2014). Genome-scale CRISPR-Cas9 knockout screening in human cells. Science *343*, 84–87.

Sohn, S.Y., Bae, W.J., Kim, J.J., Yeom, K.H., Kim, V.N., and Cho, Y. (2007). Crystal structure of human DGCR8 core. Nat. Struct. Mol. Biol. *14*, 847–853.

Townson, S.M., Dobrzycka, K.M., Lee, A.V., Air, M., Deng, W., Kang, K., Jiang, S., Kioka, N., Michaelis, K., and Oesterreich, S. (2003). SAFB2, a new scaffold attachment factor homolog and estrogen receptor corepressor. J. Biol. Chem. *278*, 20059–20068.

Truscott, M., Islam, A.B., and Frolov, M.V. (2016). Novel regulation and functional interaction of polycistronic miRNAs. RNA *22*, 129–138.

Wan, C., Tempel, W., Liu, Z.J., Wang, B.C., and Rose, R.B. (2005). Structure of the conserved transcriptional repressor enhancer of rudimentary homolog. Biochemistry *44*, 5017–5023.

Wang, Y., Luo, J., Zhang, H., and Lu, J. (2016). MicroRNAs in the same clusters evolve to coordinately regulate functionally related genes. Mol. Biol. Evol. *33*, 2232–2247.

Weng, M.T., and Luo, J. (2013). The enigmatic ERH protein: its role in cell cycle, RNA splicing and cancer. Protein Cell *4*, 807–812.

Yang, J.S., Maurin, T., Robine, N., Rasmussen, K.D., Jeffrey, K.L., Chandwani, R., Papapetrou, E.P., Sadelain, M., O'Carroll, D., and Lai, E.C. (2010). Conserved vertebrate mir-451 provides a platform for Dicer-independent, Ago2-mediated microRNA biogenesis. Proc. Natl. Acad. Sci. USA *107*, 15163–15168.

Yoda, M., Cifuentes, D., Izumi, N., Sakaguchi, Y., Suzuki, T., Giraldez, A.J., and Tomari, Y. (2013). Poly(A)-specific ribonuclease mediates 3′-end trimming of Argonaute2-cleaved precursor microRNAs. Cell Rep. *5*, 715–726.

Zeng, Y., Yi, R., and Cullen, B.R. (2005). Recognition and cleavage of primary microRNA precursors by the nuclear processing enzyme Drosha. EMBO J. *24*, 138–148.

Zhang, H., Kolb, F.A., Jaskiewicz, L., Westhof, E., and Filipowicz, W. (2004). Single processing center models for human Dicer and bacterial RNase III. Cell *118*, 57–68.

Zhang, L., Flygare, J., Wong, P., Lim, B., and Lodish, H.F. (2011). miR-191 regulates mouse erythroblast enucleation by down-regulating Riok3 and Mxi1. Genes Dev. *25*, 119–124.

STAR★METHODS

KEY RESOURCES TABLE

REAGENT or RESOURCE	SOURCE	IDENTIFIER
Antibodies		
Rabbit polyclonal anti-ERH	ThermoFisher Scientific	Cat# PA5-21388; RRID: AB_11155225
Rabbit polyclonal anti-β-Actin	Cell Signaling Technology	Cat# 4967; RRID: AB_330288
IRDye 680RD Goat anti-Rabbit IgG	Li-Cor Inc	Cat# 926-68071; RRID: AB_10956166
Bacterial and Virus Strains		
One Shot TOP10 chemically competent *E. coli*	ThermoFisher Scientific	C404003
Stable Competent *E. coli* (High Efficiency)	New England Biolabs	C3040H
Chemicals, Peptides, and Recombinant Proteins		
[γ-^{32}P] ATP	Perkin Elmer	NEG035C001MC
3′-deoxyadenosine [α-^{32}P] ATP (Cordycepin)	Perkin Elmer	NEG026250UC
TRI Reagent Solution	ThermoFisher Scientific	AM9738
Yeast RNA	ThermoFisher Scientific	AM7118
Superase-In	ThermoFisher Scientific	AM2696
GE Healthcare Hybond-NX Membrane	VWR	95038-412
ULTRAhyb-Oligo hybridization buffer	ThermoFisher Scientific	AM8663
EDC (N-(3-dimethylaminopropyl)-N0-ethylcarbodiimide)	ThermoFisher Scientific	22891
Polyethylenimine, Linear (MW 25,000)	Polysciences	23966
Polybrene	Santa Cruz Biotechnology	SC-134220
Puromycin	ThermoFisher Scientific	A1113803
Doxycycline	Takara Bio	631311
Halt Protease Inhibitor Cocktail (100 ×)	ThermoFisher Scientific	78438
RIPA Lysis and Extraction Buffer	ThermoFisher Scientific	89901
3 × FLAG peptide	Synthesized at the Biopolymers & Proteomics Core Facility at Koch Inst. (MIT)	N/A
ANTI-FLAG M2 Affinity Gel	Sigma	A2220
Strep-Tactin Superflow high capacity resin	IBA Lifesciences	2-1208-010
Critical Commercial Assays		
Lipofectamine 2000	ThermoFisher Scientific	11668019
ExpiFectamine 293 Transfection Kit	ThermoFisher Scientific	A14524
QuikChange Lightning Multi Site-Directed Mutagenesis	Agilent	210515
KAPA HiFi HotStart PCR Kit	Roche	NC0636151
Turbo DNase	ThermoFisher Scientific	AM2239
T4 PNK	New England Biolabs	M0201
Alkaline Phosphatase, Calf Intestinal (CIP)	New England Biolabs	M0290
T4 DNA ligase	New England Biolabs	M0202
T4 RNA Ligase 2, truncated K227Q	New England Biolabs	M0351
Poly(A) Polymerase, Yeast	ThermoFisher Scientific	74225Z25KU

(*Continued on next page*)

Continued

REAGENT or RESOURCE	SOURCE	IDENTIFIER
SuperScript III Reverse Transcriptase	ThermoFisher Scientific	18080044
PowerUp SYBR Green Master Mix	ThermoFisher Scientific	A25779
Micro Bio-Spin P30 gel columns	Bio-Rad	7326250
Oligo Clean & Concentrator	Zymo Research	D4060
Spin-X Centrifuge Tube Filters	Corning	CLS8162
Amicon Ultra-0.5 Centrifugal Filter Unit (100K MWCO)	Millipore	UFC510024
Amicon Ultra-4 Centrifugal Filter Unit (100K MWCO)	Millipore	UFC810024
Slide-A-Lyzer MINI device (20K MWCO)	ThermoFisher Scientific	69590
GelCode Blue Stain Reagent	ThermoFisher Scientific	24590
Pierce Silver Stain Kit	ThermoFisher Scientific	24612
Deposited Data		
Small-RNA sequencing	This paper	GEO: GSE142818
All original gels and blots	This paper; Mendeley data	https://doi.org/10.17632/fghs5z4yp4.13
Experimental Models: Cell Lines		
Human: Expi293F cells	ThermoFisher Scientific	A14527
Human: K562-dCas9-KRAB	Gilbert et al., 2014	N/A
Human: K562 cells	ATCC	CCL-243
Human: HEK293T Drosha knockout cells	Dai et al., 2016	N/A
Human: HEK293T Drosha, DGCR8 double knockout cells	Dai et al., 2016	N/A
Oligonucleotides		
See Table S2	N/A	N/A
Recombinant DNA		
pBI-CMV1	Clontech	631630
pBI-CMV1-mir144-CMV2-mir1	This paper	N/A
pBI-CMV1-mir451-CMV2-mir1	This paper	N/A
pBI-CMV1-mir144∼451-CMV2-mir1	This paper	N/A
pBI-CMV1-mir451-CMV2-mir1∼144	This paper	N/A
pBI-CMV1-mir451∼144-CMV2-mir1	This paper	N/A
pBI-CMV1-mir451∼451-CMV2-mir1	This paper	N/A
pBI-CMV1-mir125-CMV2-mir1	This paper	N/A
pBI-CMV1-mir125∼451-CMV2-mir1	This paper	N/A
pBI-CMV1-mir181b-1-CMV2-mir1	This paper	N/A
pBI-CMV1-mir181b-1∼125-CMV2-mir1	This paper	N/A
pBI-CMV1-mir374b-CMV2-mir1	This paper	N/A
pBI-CMV1-mir421-CMV2-mir1	This paper	N/A
pBI-CMV1-mir374b∼421-CMV2-mir1	This paper	N/A
pBI-CMV1-mir144m1∼451-CMV2-mir1	This paper	N/A
pBI-CMV1-mir144m2∼451-CMV2-mir1	This paper	N/A
pBI-CMV1-mir144m3∼451-CMV2-mir1	This paper	N/A
pBI-CMV1-mir144m4∼451-CMV2-mir1	This paper	N/A
pBI-CMV1-mir144m5∼451-CMV2-mir1	This paper	N/A

(*Continued on next page*)

Continued

REAGENT or RESOURCE	SOURCE	IDENTIFIER
pBI-CMV1-mir144[309 nt]∼451-CMV2-mir1	This paper	N/A
pBI-CMV1-mir144[909 nt]∼451-CMV2-mir1	This paper	N/A
pBI-CMV1-mir144[3072 nt]∼451-CMV2-mir1	This paper	N/A
pU6-sgRNA EF1Alpha-puro-T2A-BFP	Gilbert et al., 2014	Addgene #60955
pU6-mir144 EF1Alpha-puro-T2A-BFP	This paper	N/A
pU6-mir451 EF1Alpha-puro-T2A-BFP	This paper	N/A
pU6-mir144∼451 EF1Alpha-puro-T2A-BFP	This paper	N/A
pU6-sgRNA EF1Alpha-puro-T2A-BFP.ERH1	This paper	N/A
pU6-sgRNA EF1Alpha-puro-T2A-BFP.ERH2	This paper	N/A
pLentiCRISPRv1	Shalem et al., 2014	N/A
pLentiCRISPRv1.mir144_KO	This paper	N/A
pLentiCRISPRv1.linker_KO	This paper	N/A
pLentiCRISPRv1.mir451_KO	This paper	N/A
pCK-Drosha-FLAG	Han et al., 2004	N/A
pCK-Drosha(UniProt)-FLAG	This paper	N/A
pCK-Drosha(UniProt)-FLAG-mEGFP	This paper	N/A
pCK-D390(UniProt)-FLAG	This paper	N/A
pCK-D390TN(UniProt)-FLAG	This paper	N/A
pFLAG/HA-DGCR8	Landthaler et al., 2004	Addgene #10921
pNoTag-DGCR8	This paper	N/A
Software and Algorithms		
ImageQuant TL (v8.1.0.0)	GE Healthcare	N/A
FASTX-toolkit	http://hannonlab.cshl.edu/fastx_toolkit	N/A
GraphPad Prism	GraphPad software	N/A
TIDE: Tracking of Indels by DEcomposition	https://tide.deskgen.com	N/A
Image Studio	LI-COR	N/A
Other		
Small-RNA sequencing protocol, step-by-step	Fang and Bartel, 2015	http://bartellab.wi.mit.edu/protocols.html
Small-RNA northern protocol, step-by-step	Fang and Bartel, 2015	http://bartellab.wi.mit.edu/protocols.html
CRISPR knockout guide cloning protocol, step-by-step	Shalem et al., 2014	http://genome-engineering.org/gecko/wp-content/uploads/2013/12/lentiCRISPRv2-and-lentiGuide-oligo-cloning-protocol.pdf
CRISPRi guide cloning protocol, step-by-step	Gilbert et al., 2014	https://weissmanlab.ucsf.edu/CRISPR/CRISPR.html

LEAD CONTACT AND MATERIALS AVAILABILITY

Further information and requests for resources and reagents should be directed to and will be fulfilled by the Lead Contact, David Bartel (dbartel@wi.mit.edu).

EXPERIMENTAL MODEL AND SUBJECT DETAILS

All cells were cultured at 37°C with 5% CO_2. Expi293F Cells were cultured in Expi293 Expression Media (ThermoFisher Scientific) with shaking at 125 rpm. K562 cells were cultured in RPMI 1640 Media (ThermoFisher Scientific) with 10% FBS (Takara). HEK293FT cells, Drosha-knockout and Drosha, DGCR8 double-knockout HEK293T cells were cultured in DMEM (ThermoFisher Scientific) with 10% FBS (Takara). Each of these cell lines is of female origin.

METHOD DETAILS

Plasmid construction

All plasmids used for Pol II-dependent miRNA overexpression, and for making T7 transcription templates of the miR-451 variants used in *in vitro* assays, were derived from pBI-CMV1 (Clontech). Query miRNA hairpins with flanking sequences were inserted between the NotI and HindIII restriction sites under the CMV1 promoter. The control miR-1 hairpin (in one case including downstream miR-144 hairpin) with flanking sequences was inserted between the BglII and PstI sites under the CMV2 promoter. The inserted sequences with restriction sites were either PCR amplified using KAPA HiFi DNA Polymerase (KAPA Biosystems) or synthesized as gBlocks (IDT), digested, and ligated to the pre-digested vector backbone. For the miR-451∼451 construct, a synthesized gBlock of the miR-451 hairpin with flanking sequences was cloned between the PvuII and NotI sites of the pBI-miR-451 expression plasmid. To make constructs that had additional linker sequences between miR-144 and miR-451 hairpins, we PCR amplified exogenous sequences from nanoLuc (309 nt and 909 nt linker lengths) or the yeast gene *ski2* (3072 nt linker length), adding KpnI and SbfI sites to the ends, and cloned them into the construct that expressed miR-144∼451, which had been reverse-PCR amplified to introduce the KpnI and SbfI sites. To construct miR-144 hairpin variants (m1–5), we introduced mutations on primers that were used to reverse-PCR amplify and linearize the miR-144∼451 plasmid; the linearized plasmids were then circularized by T4 Polynucleotide Kinase and T4 DNA ligase (NEB). To express miRNA hairpins under the U6 promoter, we PCR amplified corresponding miRNA hairpins and flanking sequences and cloned between BstXI and XhoI sites in the CRISPRi vector (pU6-sgRNA EF1Alpha-puro-T2A-BFP) from the Weissman lab (Addgene #60955).

Lentiviral vectors that were used in the Cas9-mediated knockout experiments were derived from pLentiCRISPRv1 and were constructed following the protocol from the Zhang lab (http://genome-engineering.org/gecko/wp-content/uploads/2013/12/lentiCRISPRv2-and-lentiGuide-oligo-cloning-protocol.pdf) (Shalem et al., 2014). Plasmids for overexpressing Drosha were modified from pCK-Drosha-FLAG (Han et al., 2004) by introducing the following substitutions using QuikChange Multi Site-Directed Mutagenesis Kit (Agilent) to match the Drosha sequence on UniProt: P30S, V135A, G200S, L321S. A plasmid for overexpressing DGCR8 without tag was modified from pFLAG/HA-DGCR8 (Landthaler et al., 2004) (Addgene #10921). All insert sequences were verified by Sanger sequencing. The sequences of all oligonucleotides and gBlocks are listed in Table S2.

Transfection

For miRNA ectopic expression in Expi293F cells, 1.4 μg of the expression plasmid and 0.1 μg of pMAX-GFP (Lonza) were diluted in 50 μl OPTI-MEM (ThermoFisher Scientific), 4 μl of 1 mg/ml polyethylenimine (PEI, Polysciences) was diluted in 50 μl OPTI-MEM, and the diluted plasmid DNA and PEI were mixed and incubated for 15 min before adding to 1 mL of the Expi293F cells at a density of 2 million cells per ml in a 12-well tissue culture plate. Cells were harvested 36–48 h post transfection. For assessing pri-miRNA expression under the U6 promoter, 2.4 μg of the expression plasmids and 0.1 μg of pMAX-GFP were reverse-transfected into 1.5 million Drosha-knockout HEK293T cells in a 6-well tissue culture plate, using 7.5 μl Lipofectamin 2000 (ThermoFisher Scientific). Cells were harvested 36–48 h post transfection.

RNA extraction and northern blotting

Cells were washed with PBS, and total RNA was extracted using TRI Reagent (ThermoFisher Scientific) following manufacturer's protocol. A detailed protocol for small RNA blots is available at http://bartellab.wi.mit.edu/protocols/Small_RNA_Northern_Blot_Protocol_2014.pdf. For each miRNA examined, the probe hybridized to the annotated guide strand. The sequences of all probes are listed in Table S2.

RT-qPCR analysis of pri-miRNAs

Total RNA was treated with TURBO DNase (ThermoFisher Scientific) and reversed transcribed using random hexamers and SuperScript III (ThermoFisher Scientific). cDNA was assayed using Power SYBR Green PCR Master Mix (ThermoFisher Scientific) and the QuantStudio 6 Real-Time PCR system (ThermoFisher Scientific). Pri-miRNA levels were determined by the $\Delta\Delta$Ct method using *GAPDH* mRNA as the internal control. The sequences of all primers are listed in Table S2.

Cell lines with deletions in the *MIR-144∼451* locus

To target the miR-144 hairpin, the linker region, or the miR-451 hairpin, sequences corresponding to six gRNAs for each region (chosen with assistance from https://zlab.bio/guide-design-resources or http://crispor.tefor.net/) were cloned into pLentiCRISPRv1. These constructs were transfected into HEK293FT cells, together with packaging vectors expressing VPR and VSV-G (plasmid ratio = 9:8:1, gRNA vector:VPR:VSV-G), using Lipofectamin 2000 (ThermoFisher Scientific) following manufacturer's instructions.

After 72 h, the media was collected, cleared by centrifugation, and added to K562 cells at 1:1 volume ratio (final cell density at 0.2 million per ml) in 12-well tissue culture plates. Polybrene (Santa Cruz Biotechnology) was supplemented at 8 μg/ml. The plates were centrifuged at 1,200 g for 2 h at room temperature and then returned to the 37°C incubator. After 24 h, cells were washed with PBS and then selected for gRNA expression with puromycin (1 μg/ml, ThermoFisher Scientific) for ~5 days. Genomic DNAs from these polyclonal cell lines were extracted using QuickExtract DNA Extraction Solution (Lucigen), the *MIR-144~451* locus was PCR amplified, and the products were sequenced by Sanger sequencing. The genotypes were analyzed by TIDE (https://tide.deskgen.com/), which provided the information needed to choose an efficient gRNA for each target region. The polyclonal cells expressing the efficient gRNAs were then single-cell sorted to obtain clonal cell lines. Cell lines were screened by Sanger sequencing to find those that were mutant at the desired loci. The sequences of all gRNAs and PCR primers are listed in Table S2.

Lysate from cells overexpressing Microprocessor

Plasmids for overexpressing Drosha-FLAG or D390-FLAG (14.2 μg) and DGCR8 (28.4 μg) were transfected into Expi293F cells (60 million in 30 mL of media) with the spike-in pMAX-GFP (2.4 μg), using 120 μl PEI (Polysciences). After 48 h, cells were washed with PBS, and the ~0.4 mL cell pellet was resuspended in 2.25 mL reaction buffer (20 mM Tris-Cl pH 8.0, 100 mM KCl, 2 mM $MgCl_2$, 0.2 mM EDTA, 5 mM DTT, 0.3 mg/ml yeast RNA), sonicated (Fisher Scientific, with the probe model CL-18) for six rounds, performing 10 strokes (1 s on, 1 s off, Amplitude 50%) followed by a 2 min incubation on ice in each round. After clearing by centrifugation at 20,000 g for 20 min at 4°C, lysate was aliquoted, flash-frozen, and stored at − 80°C for single usage.

In vitro processing and data fitting

Pri-miRNA substrates were prepared by T7 *in vitro* transcription of PCR products in which the appropriate regions of sequenced plasmids had been amplified and the T7 promoter had been appended. The sequences of all primers are listed in Table S2. After transcription, DNA templates were digested using TURBO DNase (ThermoFisher Scientific), and RNAs were ethanol precipitated and purified on polyacrylamide urea gels. Most RNAs were 3′ end labeled using cordycepin (Perkin Elmer) and Yeast Poly(A) Polymerase (ThermoFisher Scientific), purified using the Oligo Clean & Concentrator kit (Zymo Research), and eluted in water. For internal labeling of pri-miR-144~451 (Figure 5D), the 3′ fragment was dephosphorylated by treatment with CIP, T4-PNK labeled using [γ-^{32}P] ATP (Perkin Elmer), and ligated with the 5′ fragment by splint ligation using T4 DNA ligase. The labeled substrates were quantified using the Qubit RNA Broad Range Assay kit (ThermoFisher Scientific). Each 60 μl processing reaction contained 3 μl of 0.2 μM RNA substrate (to achieve a final concentration of 10 nM), 3 μl water (or the other RNA substrate at 0.2 μM if the reaction had two substrates), and 54 μl of lysate. Lysate was preincubated at 37°C for ~3 min, and reactions were started by the addition of substrate(s). At indicated time points, 7 μl of the reaction was pipetted into 800 μl TRI reagent to stop the reaction. The substrates and processing products were extracted and resolved on 8% polyacrylamide urea gels. After drying, the radiolabel was imaged on a Typhoon FLA 7000 (GE Healthcare) and quantified by Multi Gauge (FUJI Film). Each observed rate constant was obtained by fitting all data from two or three independent time-course experiments to the equation $y = 1 - e^{-kt}$.

Purification of Microprocessor for *in vitro* processing assay

Plasmid transfections were performed as above but in larger scales using 0.6–1 × 10^9 cells (plasmid ratio of Drosha-FLAG-mEGFP:DGCR8 = 1:3). Cell pellets were resuspended in IP buffer (20 mM Tris-Cl pH 7.5, 150 mM NaCl, 0.1 mM EDTA, 0.01% NP-40, 5% glycerol, supplemented with Halt Protease Inhibitor), sonicated, cleared, and incubated with M2 anti-FLAG affinity gel (Sigma) for 2 h, washed with wash buffer (20 mM Tris-Cl pH 7.5, 300 mM NaCl, 0.1 mM EDTA, 0.01% NP-40, 5% glycerol), and eluted using 3 × FLAG peptide in IP buffer. Eluates were concentrated using Amicon Ultra-0.5 (100K MWCO), dialyzed against storage buffer (20 mM Tris-Cl pH 8.0, 100 mM KCl, 2 mM $MgCl_2$, 0.2 mM EDTA, 5 mM DTT) using Slide-A-Lyzer MINI device (20K MWCO), aliquoted, flash-frozen, and stored at − 80°C for single use.

Purification of Microprocessor for ERH identification

Plasmid transfections were performed at large scale with a plasmid ratio of D390-TN-FLAG:DGCR8:GFP = 1:8:1. Plasmid transfection for Figure 7D was performed with PEI, as above, whereas transfection for Figure 7E was performed using the ExpiFectamine 293 Transfection Kit (ThermoFisher Scientific), following the manufacturer's manual. Cell pellets were resuspended in IP buffer, sonicated, cleared, and incubated with M2 anti-FLAG affinity gel (Sigma) for 2 h, washed with high-salt wash buffer (20 mM Tris-Cl pH 7.5, 500 mM NaCl, 0.1 mM EDTA, 0.01% NP-40, 5% glycerol), eluted with 3 × FLAG peptide in IP buffer, and concentrated using Amicon Ultra-4 (100K MWCO). For purification on the basis of pri-miRNA affinity, concentrated M2 eluate was incubated with 5′-desthiobiotin labeled artificial pri-miRNA in IP buffer supplemented with 1 mM ATP and 5 mM $MgCl_2$ at room temperature for 12 min, and then incubated with Strep-Tactin resin (IBA) for 30 min, washed with binding buffer (20 mM Tris-Cl, pH 7.5, 150 mM NaCl, 5 mM $MgCl_2$, 0.01% NP40, 5% Glycerol, 1 mM TCEP), and eluted with 5 mM biotin in elution buffer (20 mM Tris-Cl, pH 7.5, 150 mM NaCl, 5 mM MgCl2, 0.01% NP-40, 1 mM TCEP). Approximately 5% of the preparation was loaded on the gel in Figure 7D. For gel-filtration analysis, Strep-Tactin eluate was loaded on a Superdex 200 Increase 10/300 GL column (GE Healthcare) in elution buffer, run at 0.5 ml/min and collecting each 0.5 mL fraction. Approximately 2% of the fraction was loaded on the gel in Figure 7E. The sequence of the artificial pri-miRNA is listed in Table S2.

CRISPR interference knockdown of ERH

Doxycycline-inducible polyclonal cell lines were made as described (Gilbert et al., 2014) and using lentivirus as above. To induce knockdown, 0.05 μg/ml doxycycline was added to the media. The sequences of all gRNAs and PCR primers are listed in Table S2. For the western blot used to confirm ERH knockdown, cells were pelleted 3 d post induction, lysed in RIPA Buffer (ThermoFisher Scientific), and the whole-cell lysates were separated by SDS-PAGE, followed by transfer to a PVDF membrane. The membrane was blocked using 5% non-fat milk in PBST (0.05% Tween-20 in PBS) at room temperature for 15 min, incubated with primary antibodies (1:500 to 1:2000 dilution) in PBST at 4°C overnight, washed in PBST at room temperature three times (5 min each), and incubated with the secondary antibody in dark for 1 h at room temperature. After washing in PBST at room temperature three times (5 min each), the membrane was imaged on an Odyssey CLx (LI-COR), and analyzed using Image Studio (LI-COR).

Small-RNA sequencing and analysis

A detailed protocol for making small-RNA sequencing libraries is available at http://bartellab.wi.mit.edu/protocols/Small_RNA_library_prep_2017.pdf. After adaptor trimming and quality filtering (fastq_quality_filter, -q 30 -p 100), a read was assigned to a miRNA if it contained an exact match to the first 18 nt of the miRNA. An annotation of miRNA clusters (miRNA genes < 10 kb apart) was derived from the chromosomal positions curated on MirGeneDB (Fromm et al., 2020). If a cluster contained at least two miRNAs with more than 100 reads from each of the control replicates, the expression change (ERH knockdown/control) of each miRNA in the cluster was compared with the geometric average of the expression change of other members of its cluster. The t test was used to calculate the statistical significance for each miRNA. Read counts and relative expression changes for all clustered miRNAs passing our expression cutoff are listed in Table S1.

QUANTIFICATION AND STATISTICAL ANALYSIS

GraphPad Prims 8 was used to generate graphs and perform statistical analysis. Statistical parameters including the value of *n*, statistical test, and statistical significance (*p* value) are reported in figures and their legends. For plasmid-based miRNA overexpression experiments, replicates refer to transfections performed with separate transfection mixtures (on the same or different days). For studies involving clonal cell lines, replicates refer to samples derived from different cell lines. For *in vitro* processing assays, replicates refer to reactions performed on different days. No statistical methods were used to predetermine sample size.

DATA AND CODE AVAILABILITY

The accession number for the sequencing data reported in this paper is GEO: GSE142818.